Journal of Food Engineering 292 (2021) 110370

Contents lists available at ScienceDirect

Journal of Food Engineering

journal homepage: http://www.elsevier.com/locate/jfoodeng

Multiresponse kinetic modelling of the formation, release, and degradation of allyl isothiocyanate from ground mustard seeds to improve active packaging

Nur Alim Bahmid [a,b], Jenneke Heising [a], Matthijs Dekker [a,*]

[a] Food Quality and Design Group, Wageningen University and Research, P.O. Box 17, 6700, AA, Wageningen, the Netherlands
[b] Agricultural Product Technology Department, Universitas Sulawesi Barat, Majene, 91412, Indonesia

ARTICLE INFO

Keywords:
Allyl isothiocyanate
Mustard seeds
Multiresponse kinetic
Mechanistic modelling
Mass transfer
Antimicrobial packaging

ABSTRACT

This study aims to describe allyl isothiocyanates (AITC) formation from enzymatic sinigrin hydrolysis in ground mustard seeds and its release and degradation in the headspace using multiresponse kinetics modelling. The mechanistic modelling of the steps involved in the packaging system consists of a set of ordinary differential equations established from bio (chemical) reaction models combined with mass transfer models. The estimated parameters consist of the accessible sinigrin fraction, rate constants of sinigrin hydrolysis, AITC degradation in the particles and headspace, and its mass transfer coefficient. The model provides a good fit to experimental results and confirms the proposed mechanism of the AITC formation, degradation, and release inside the packaging system. Fat content has significant effects on AITC formation and release rate constants, while particle sizes significantly affect accessible sinigrin in the particles. These results give an understanding of AITC's controlled release by manipulating the mustard properties to optimize antimicrobial packaging designs.

1. Introduction

Antimicrobial packages are currently being developed by the food industries for shelf life extension of food products by preventing the spoilage bacteria to grow at its food surface (Reyes-Jurado et al., 2019). Antimicrobial packages contain compounds that can be slowly released from antimicrobial carriers to food products with direct surface-food contact transfer or indirect headspace transfer (Wong et al., 2020). For indirect contact, the concentration of volatile compounds in the headspace determines the microbial growth rate in the food (Kurek et al., 2017). Therefore, controlling the release rate of the compounds to the headspace to retain sufficient concentrations has a major impact in effectively preventing bacterial growth to reach the desired product shelf life (Lorenzo et al., 2014; Quintavalla and Vicini, 2002).

Allyl isothiocyanate (AITC) is acknowledged as a strong antimicrobial agent and can be formed from the enzymatic hydrolysis of sinigrin, which is the main glucosinolate in mustard seeds (Reyes-Jurado et al., 2019). Once the cells of the mustard seeds are disrupted, e.g. during the grinding process and fat extraction, myrosinase hydrolyzes the sinigrin upon moisture exposure to yield AITC (Hanschen et al., 2018; Okunade et al., 2015). The formed AITC can be subsequently partitioned to phases with different stability; fat phase of the seeds (most stable), headspace (slightly stable), or aqueous phase (unstable). Bahmid et al. (2020) reported that AITC amount released from the ground mustard seeds still containing fat was lower than the AITC release from defatted ground mustard seeds (0% fat). The results indicate that the AITC prefers to move into the fat phase of the mustard particles rather than into the packaging headspace (Dai and Lim, 2014). To understand the AITC partition and stability, the kinetics of the release and degradation of AITC taking place in the seeds and headspace of the package needs to be evaluated by developing such a kinetic model.

Multiresponse modelling could be used as a powerful tool for describing physical and chemical processes using multiresponse data, such as multiple compounds involved in chemical reactions (Boekel, 2009; Verkempinck et al., 2019). This model approach is used to estimate parameters more accurately and is considered as a more comprehensive assessment of a proposed mechanistic model, compared to single response modelling (Quintas et al., 2007; Ziegel and Gorman, 1980). Some examples of studies using multiresponse modelling are on the understanding of the complex reaction mechanisms of lipid digestion (Verkempinck et al., 2019), caramelization, and Maillard reactions (Goncuoglu Tas and Gokmen, 2017; Kocadağlı and Gökmen, 2016). Applying multiresponse kinetic modelling in food packaging, is still

* Corresponding author.
E-mail address: matthijs.dekker@wur.nl (M. Dekker).

https://doi.org/10.1016/j.jfoodeng.2020.110370
Received 13 July 2020; Received in revised form 7 September 2020; Accepted 5 October 2020
Available online 7 October 2020

Nomenclature/abbreviation

A	= the surface area of the interface mustard particles (m^2)
A_e	= gas chromatographic peak area of AITC in the headspace at equilibrium
AITC	= Allyl isothiocyanates
$AITC_g$	= concentration of AITC in the headspace (mol/m^3)
$AITC_s$	= concentration of AITC in the particles (mol/m^3)
$AITC_s^i$	= concentration of AITC in the interface of the particles (mol/m^3)
C_e	= equilibrium AITC concentration in the emulsion
C_o	= initial concentration of AITC in the seeds (mol/m^3)
d	= diameter of ground mustard seeds/mustard particles (m)
f_0	= proportional factor ($A_e = f_0 \cdot C_e$)
fat	= fat content in the seeds (%)
GC-FID	= Gas Chromatoghraphy – Flame Ionization Detector
H_2O	= concentration of added water in-ground seeds (mol/m^3)
HPLC	= High-Performance Liquid Chromatography
k_1	= rate constant of sinigrin degradation and AITC formation (h^{-1})
k_2	= rate constant of AITC degradation in the mustard particles (h^{-1})
k_3	= rate constant of AITC degradation in the headspace (m^3/mol/h)
$K_{s/g}$	= equilibrium partition coefficient ground mustard seeds and headspace (dimensionless)
MIC	= Minimum Inhibitory Concentration
m_s	= mass of mustard particles (g)
m_t	= mass transfer coefficient from mustard particles into headspace (m/h)
N	= molar flux (mol/m^2h)
p_g	= breakdown products in the headspace
p_s	= breakdown products in the mustard particles
Sin_a	= concentration of accessible in mustard particles sinigrin (mol/m^3)
Sin_i	= concentration of inaccessible sinigrin in mustard particles (mol/m^3)
Sin_{tot}	= concentration of total sinigrin in particles (mol/m^3)
t	= time (h)
V_g	= volume of headspace (m^3)
V_s	= volume of mustard particles (m^3)
V_{vi}	= volume of glass vial (m^3)
β	= phase volume ratio of headspace to the emulsion
ρ_s	= density of mustard particles (g/m^3)

limited, whereas food packaging has a high complexity including mass transfer/migration of compounds through the package, between the packaging material and the packaged food and reactions with food components.

A single modelling approach was applied to understand the release of compounds from a film in an active antimicrobial package by Kurek et al. (2017). The single response of mathematical model used to describe the AITC release from the encapsulation of β-cyclodextrin (β-CD) from a polymeric matrix did not include the possible reaction in the film or the headspace, or absorption of the volatile in the packaged (model) food. Ignoring these mechanisms, which will also change the concentration in the film and headspace, will have led to less accurate predictions of the model parameters. A multiresponse kinetic model can, therefore, be a novel way to describe those changes of compound concentration in the whole packaging system, which benefits the understanding of the reactions and mass transfer involved in the packaging system in an integrated way.

The multiresponse kinetic modelling approach in this mechanistic study aims to describe the formation, release, and degradation of the AITC in the packaging system. The experimental data of sinigrin degradation, concentration AITC in mustard particles, and headspace investigated from our previous study (Bahmid et al., 2020) were used. The fits of the developed kinetic model to the measured data of the sinigrin and AITC concentration in each phase of the package were evaluated to determine whether the established model was able to accurately describe degradation and release of AITC. A better understanding of the reactions and mass transfer in the packaging system could help to optimize the mustard seeds properties and packaging design to effectively control the AITC release in antimicrobial packaging.

2. Theoretical considerations

Sinigrin degradation is initiated upon tissue and cell damage in the mustard seeds (Okunade et al., 2015). Sinigrin is located in protein bodies or vacuoles of S-cells and the hydrolyzing enzyme myrosinase is located in different compartments, called myrosin cells (Kissen et al., 2009; Nakano et al., 2014; Stauber et al., 2012; Torrijos et al., 2019). Once the tissue is disrupted by physical disruption or fat extraction, myrosinase instantaneously hydrolyzes sinigrin to form AITC in the presence of water (Dekker et al., 2009; Tetteh et al., 2019; Xiao et al., 2019). This mechanism of hydrolysis of sinigrin is called the "mustard oil bomb theory" (Stauber et al., 2012). Lüthy and Matile (1984) developed this theory for the subcellular organization of the glucosinolate-myrosinase system in horse-radish roots (*Sinapsis alba*). This theory explains the stability of the glucosinolate-myrosinase system with a different compartment of the substrate and enzyme. The theory was then critically assessed by Kissen et al. (2009) that clarified that the glucosinolate hydrolysis by myrosinase happened only in the case of tissue damages.

The accessible sinigrin is enzymatically hydrolyzed by myrosinase upon the addition of water to yield AITC in the ground mustard seeds. In the mustard particles, the formed AITC can be degraded due to the water added to the packaging system. The water attacks the sulfhydryl groups of AITC to form other compounds (Encinas-Basurto et al., 2017; Olaimat and Holley, 2016). At the same time, the volatile AITC also partitions into the headspace. From the headspace, the AITC has an antimicrobial effect on the food product in the package. In the headspace, AITC can react with moisture to form other compounds as occurred in the mustard particles as well. These reactions and mass transfer pathways are schematically depicted in Fig. 1a.

Fig. 1b shows the release of AITC from mustard particles into headspace, which can be specifically described by the theory of mass transfer from a solid to a gas (Harrison et al., 2006). In the mustard particle phase, AITC diffuses to the interface and is transferred from the ground mustard seeds, across the interface, into the headspace through unsteady state molecular diffusion. The main resistance of this transfer will be in the outer surface layer of the mustard seed particles. This mass transfer occurs until reaching the equilibrium in concentration between the ground mustard seeds and headspace.

3. Methods

3.1. Sample preparation

Mustard seeds were freeze-dried (Christ Alpha 1–4 LD plus) and then ground by using a milling machine (Fritsch; Pulverisette 14). The ground particles were sieved (Hosokawa Alpine Air Jet sieve 200 Ls) in different particle sizes (50–100, 200–315, 400–500 and 630–800 μm) and then d efatted using soxhlet extraction till intended fat content

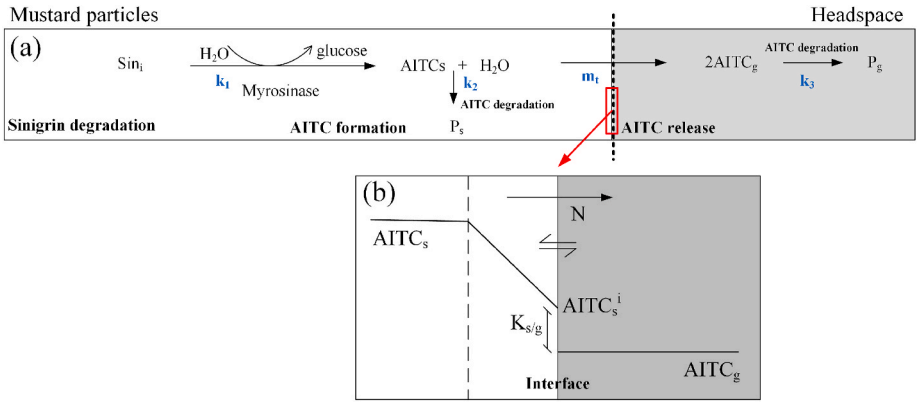

Fig. 1. Schematic representation of allyl isothiocyanate (AITC) formation in mustard particles (white area) and AITC release in the headspace (grey area) **(a)** proposed reaction pathways on multiresponse modelling procedures, and **(b)** the schematic presentation of mass transfer of released AITC from the mustard seed particles into the headspace. N is molar flux, $k_{1\text{-}3}$ is the degradation rate constant of each phase, P_s and P_g are breakdown products of AITC in the solid and gas phase respectively, $K_{s/g}$ is the partition coefficient, and m_t is interfacial mass transfer.

(29.1%, 17.1%, 2.8%, and 0.0%) were reached. Mustard particles (0.16 g) were put inside the Duran bottles (10 mL) and rehydrated with 0.132 mL of Milli-Q water (ratio (w/v); 1:0.825) as shown in Fig. 2. The samples were stored at 20 °C for 48 h and sinigrin and AITC were measured at certain time intervals.

3.2. Sinigrin and AITC measurement

Sinigrin ($C_{10}H_{16}KNO_9S_2$; 397.46 g/mol) and AITC (C_4H_5NS; 99.15 g mol^{-1}) concentration in the mustard particles and AITC in the headspace were determined using the method described by Bahmid et al. (2020). The analysis of sinigrin and AITC in the ground mustard seeds was done by extraction followed by High-Performance Liquid Chromatography (HPLC; Thermo Scientific; UHPLC + focused Dionex Ulti-Mate 3000) according to reported by Oliviero et al. (2012) with minor adjustments. The concentration of sinigrin in mustard particles was calculated with the help of glucotropaeolione as an internal standard and the relative response factor (RRF) of sinigrin (1.053). The AITC concentration in the mustard particles was quantified by the curve of the calibration standards of pure AITC (Allyl isothiocyanate purchased from Sigma Aldrich Chemie GmbH, 97%).

Analysis of AITC in the headspace was performed using Gas Chromatoghraphy – Flame Ionization Detector (GC-FID; Thermo-Scientific, Focus GC) and autosampler (Thermo-Scientific, TriPlus Autosampler) for AITC in the headspace as described by Bahmid et al. (2020). The calibration was done with pure AITC dissolved in Hexane (n-Hexane PEC grade, Actu-All chemicals), with the range of used concentrations 1 ppm–250 ppm.

Data (mol compounds in liter volume of mustard particles or headspace) for modelling the sinigrin degradation and AITC release in the

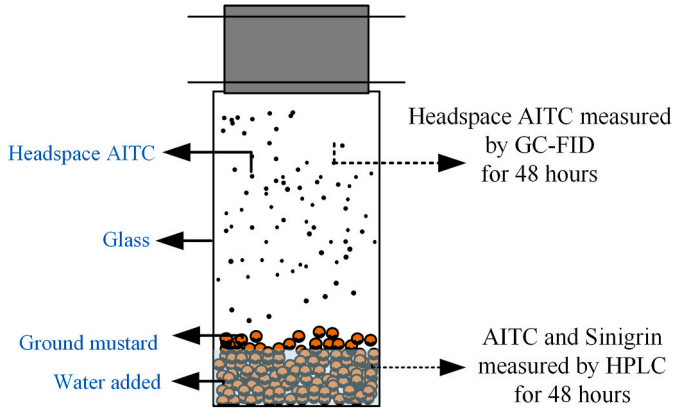

Fig. 2. The model system used to measure the allyl isothiocyanate (AITC) release in the gas phase.

headspace were collected by sampling every 3 h for 48 h in mol/m^3. Data for modelling AITC remaining in the mustard particles were collected by sampling at 0, 24, and 48 h. Each dataset was obtained using duplicate samples and expressed as the mean values ± standard deviations (SD).

3.3. Determination of the partition coefficient of AITC

The partition coefficient ($K_{s/g}$), the concentration ratio of AITC in the immiscible phase to the headspace as expressed in Equation (1), was measured using the method modified from Zhang et al. (2010).

$$K_{s/g} = \frac{AITC_s}{AITC_g} \tag{1}$$

where $AITC_s$ and $AITC_g$ are the concentrations of AITC in the immiscible phase and headspace, respectively.

To investigate the effect of fat content in mustard particles on $K_{s/g}$, emulsions with different oil (mustard oil extract) content (0, 2.8, 17.1, and 29.1%) were studied as (model) ground seeds. The oil was mixed with Milli-Q and 0.5% of tween 20 as an emulsifier with an Ultra-turrax (IKA Werke GmbH & Co. KG) at 9500 rpm min^{-1} within 2 min. The unstable emulsion was subsequently homogenized using a homogenizer (Delta Instruments) for 10 min at 120 bar. Afterward, AITC (100 mg/L) was added to the emulsions. Different volumes (1, 2, 3, 4, and 5 mL) of the emulsion were poured into 20 mL vials and immediately sealed gastightly. The samples were stored at 20 °C for 3 h to reach equilibrium partition between emulsion and headspace. The method used to perform AITC measurement using GC-FID is described in a previous publication (Bahmid et al., 2020). The partition coefficient ($K_{s/g}$) of AITC between emulsion and headspace was determined according to phase ratio variation (PRV) method (Zhang et al., 2010), which is the relationship of $K_{s/g}$, β, and the peak area (A_e) as expressed below;

$$\frac{1}{A_e} = \frac{K_{s/g}}{f_o C_o} + \frac{1}{f_o C_o}\beta \tag{2}$$

where f_0 is a proportional factor ($A_e = f_0 \cdot C_e$), and C_o and C_e are the initial concentration of AITC in the seeds and the equilibrium AITC concentration in the emulsion, respectively; A_e is gas chromatographic peak area of AITC in the headspace at equilibrium; β is the phase volume ratio of headspace to the emulsion. The value of $K_{s/g}$ can be directly calculated from the ratio of the y-intercept to the slope of the regression line in the plot of 1/Ae versus β (Zhang et al., 2010).

3.4. Development of the kinetic model

The mathematical model was restricted to (bio)chemical reactions, solid-gas equilibria, and physical mass transfer processes. It consists of a combination of differential equations, equilibria, and mass balances for

both the mustard particles and headspace phases. The following assumptions were stated;

1. All hydrolyzed sinigrin is converted in AITC on a molar basis.
2. The mass transfer takes place from the mustard particles phase to the gaseous phase, the mustard particles are loosely packed and the surface area of each particle is in contact with the gaseous phase.
3. The mass transfer to the gaseous phase is described with the stagnant film model. The conditions justify that the mass transfer in the gaseous phase can be assumed not to be a limiting factor.
4. The mustard particles are considered to be one phase, no separate aqueous, solid, and fat sub-phases are considered in the model.

The AITC formation by sinigrin hydrolysis catalyzed by myrosinase can be described by a first-order reaction (Hanschen et al., 2018). Part of the sinigrin can be in inaccessible parts of the mustard seeds that were not damaged by the grinding process. Therefore, this inaccessible sinigrin needs to be included in the first-order reaction to describe well the mechanism of sinigrin hydrolysis. The initial hydrolysis of accessible sinigrin fraction leads to the following differential equation for fractional conversion first-order kinetics;

$$\frac{d[Sin_{tot}]}{dt} = -k_1\,[Sin_a] = -k_1\,[Sin_{tot} - Sin_i] \tag{3}$$

where Sin_{tot} is the concentration of total sinigrin in particles (mol/m^3), Sin_i and Sin_a are the concentration of inaccessible and accessible sinigrin (mol/m^3) respectively, t is degradation time (h) and k_1 is the rate constant of sinigrin degradation and AITC formation (h^{-1}). The formation (f) of AITC in the mustard particles is subsequently described by:

$$\left.\frac{d[AITC_s]}{dt}\right|_f = k_1\,[Sin_a] = k_1\,[Sin_{tot} - Sin_i] \tag{4}$$

where $AITC_s$ is the concentration of AITC volatiles (mol/m^3) within the mustard particles.

The formed AITC can either be transferred to the headspace or degrade in the mustard particle. The AITC transfer to the headspace can be calculated from the penetration theory and the equilibrium constant (Harrison et al., 2006). The transfer to the headspace is determined by the mass transfer coefficient (m_t). From the theory, the mass transfer across the interface can be described by the following equation (Backhurst and Harker, 2001);

$$N = -m_t\,[AITC_s^i - AITC_s] \tag{5}$$

where N is molar flux (mol/m^{2}h), m_t is the mass transfer coefficient (m/h). $AITC_s^i$ and $AITC_s$ are the concentration of AITC volatiles at the interface (mol/m^3) and within the mustard particles (mol/m^3) respectively. As N is an unknown variable, the molar flux in Eq. (5) is integrated into the mass transfer rate (m_t) of AITC in the solid and headspace described by the following equations:

$$\left.\frac{dAITC_s}{dt}\right|_{mt} = -\frac{m_t\,A}{V_s}\,[AITC_s - AITC_g\,K_{s/g}] \tag{6}$$

$$\left.\frac{dAITC_g}{dt}\right|_{mt} = \frac{m_t A}{V_g}\,[AITC_s - AITC_g\,K_{s/g}] \tag{7}$$

where t is time (h); AITC and V are AITC concentrations and volume of each phase (m^3), respectively, and the subscripts s and g denote seed particles and gas phases, respectively.

The AITC can simultaneously be degraded in mustard particles and packaging headspace. Hydroxyl groups (e.g. from water) attack sulfhydryl groups of AITC to generate another compound, e.g. allyldithiocarbamate and pentasulfide (Tsao et al., 2000; Weerawatanakorn et al., 2015). As the amount of added water is in large excess and hardly changes over time during sinigrin hydrolysis, the mechanism of the AITC degradation in mustard particles can be described with the pseudo-first-order kinetics (Jiang et al., 2006). Yet the amount of water present in mustard particles is known, so the AITC degradation can be described by the following kinetic model equation:

$$\left.\frac{d[AITC_s]}{dt}\right|_{ds} = -k_2\,[AITC_s]\,[H_2O] \tag{8}$$

In the headspace also AITC degradation takes place due to the presence of water vapor as shown later in the results and discussion, was best described by a second-order reaction:

$$\left.\frac{d[AITC_g]}{dt}\right|_{dg} = -k_3\,[AITC_g]^2 \tag{9}$$

where k_2 and k_3 in m^3/mol.h are the rate constants of AITC degradation in the seeds and headspace, respectively, and H_2O is the amount of water per volume of the seeds (mol/m^3).

3.5. Multiresponse kinetic modelling

The proposed pathway (Fig. 1a) consists of three responses to the experimental data; sinigrin concentration in the mustard particles, AITC concentration in mustard particles, and the headspace. Those three responses were estimated using a set of differential equations of mass transfer and reaction enumerated in Eq. (10)-(12).

$$\left.\frac{d[Sin_{tot}]}{dt}\right|_{sum} = \frac{d[Sin_{tot}]}{dt} \tag{10}$$

$$\left.\frac{d[AITC_s]}{dt}\right|_{sum} = \left.\frac{d[AITC_s]}{dt}\right|_f + \left.\frac{dAITC_s}{dt}\right|_{mt} + \left.\frac{d[AITC_s]}{dt}\right|_{ds} \tag{11}$$

$$\left.\frac{d[AITC_g]}{dt}\right|_{sum} = \left.\frac{dAITC_g}{dt}\right|_{mt} + \left.\frac{d[AITC_g]}{dt}\right|_{dg} \tag{12}$$

These three differential equations were simultaneously fitted to the experimental data. The estimated parameter values consist of the inaccessible sinigrin fraction (Sin_1), rate constants (k_1, k_2, and k_3), and mass transfer coefficients (m_t). These parameters were estimated by multiresponse non-linear regression with the determinant criterion (Boekel, 2009) using Athena Visual Studio software (v.14.2) (AthenaVisual Inc.). In the parameter estimation solver control panel, standard options were used; the convergence criterion (= 0.01), the maximum number of iterations (=30), estimation solver options (non-linear least-squares, gradient calculation (forward differences scheme) and relative perturbation step size (10^{-3}). In total 41 parameters were estimated based on 1836 triplicate measurements from 17 experiments with 36 responses giving 612 data points to fit by the model. The goodness of fit of the kinetic models was then evaluated by examining the generated size and distribution of the residuals, the R-square of predicted vs observed data, and the standard deviations and correlations of the parameters.

The degradation rate in the headspace (k_3) was assumed to be independent of the fat content and particle size. The degradation rate in the particles (k_2) was assumed only to be independent of the particle size. The dependency of the partition coefficient ($K_{s/g}$) on the fat content of the particles was taken from the experimental determination explained in section 3.3. The initial concentrations (shown in Table A1 and A2 in Supplementary data) were set equal to the observed initial concentrations of sinigrin and AITC in the non-hydrated mustard particles, while the initial concentration in the headspace was set equal to zero. Parameters and constants used in the modelling with known values are given in Table A3 in Supplementary data.

3.6. Statistical analysis

Significant differences were evaluated to investigate the effects of

particle sizes and fat content on parameter estimates. Statistical significance ($p < 0.05$) was evaluated based on the method developed by Julious (2004) using the confidence intervals around individual means of the parameter estimates to assess statistical significance between two means.

4. Results and discussion

4.1. Partition coefficient ($K_{s/g}$)

The $K_{s/g}$ was thus calculated from the relationship as expressed in Eq. (2) and summarized in Fig. 3. The phase ratio variation (PRV) method used to calculate $K_{s/g}$ was depicted in Figure A2 in Supplementary Materials. The volume ratio (β) was linearly proportional with the $1/A_o$ in all different samples, which shows a good relationship between β and $1/A_o$ with R-square > 0.95.

The calculated value of $K_{s/g}$ significantly and linearly increased in the emulsion with higher oil content, as shown in Fig. 3 ($p < 0.05$). The emulsion containing over 17.1% fat content suddenly reduced the volatility of AITC in the headspace, in which the $K_{s/g}$ value of emulsion containing 29.1% fat was ten times higher than that of the emulsion containing 17.1% fat. It indicates that the higher fat content more effectively suppressed the volatility of the AITC in the headspace. The $K_{s/g}$ value of emulsion with 29.1% mustard oil (1992.7 ± 9.6) is in line with the value observed by Zhang et al. (2010) using 30% canola oil, which was 1962.9 ± 502.4. Furthermore, the linear increase of $\log_{10} k_{s/g}$ value indicates that AITC has a higher affinity for the bigger volume of fat phase in an emulsion (Keppler et al., 2018) and the low value of $K_{s/g}$ for the low-fat contents indicated the high volatility of AITC in an increase in water volume in the emulsion. These results are a useful parameter for the developed multireponse kinetic modelling.

4.2. Mechanistic multiresponse model

In Fig. 4, the multiresponse model in Eq. (10)-(12) describe observed data of sinigrin and AITC concentrations in the headspace well, including AITC concentration in the mustard particles (Figure A3. Supplementary Materials). Linear regression of the predicted vs observed data plot provided slopes very close to 1.0 (Fig. 5).

There are some considerations on the assessment of the goodness of fit. Fig. 5a shows several horizontal clustering of data, which indicates very similar predicted data while there is considerable fluctuation in the observed data. These predicted data were the result of the fractional conversion first-order kinetics, in which the same predicted data indicated the minimum value of sinigrin fraction accessed by myrosinase, while there is still experimental variation around these values. In Fig. 5b, the predicted data of AITC in the headspace has two overestimated points at high concentration. These data points are from the observed data of the defatted particles with sizes of 400–500 μm. The results of this particle size show an unexpected and peculiar result which caused a very high standard deviation in the parameter estimates (Table 2) for this sample, compared to the other particle sizes. As discussed in our previous study (Bahmid et al., 2020), the unexpected data shows fast hydrolysis, possibly due to the capillary forces being higher for the microstructure of this particular size, to completely degrade the sinigrin. In addition, the model did not satisfactory fit the peak value (underestimated) and the degradation rate (overestimated) of the measured data of headspace AITC concentration (Fig. 4f), whereas the model did perform well on the sinigrin concentration. These deviations were observed for the bigger mustard particles (400–500 and 630–800 μm) in the 29.1%-fat particles releasing low amounts of AITC. A possible reason is that at low AITC concentration in the gaseous phase and high amounts of fat in the mustard particles, the equilibrium between headspace and mustard particles is competing with the equilibrium between the aqueous and fat phase inside the mustard particles (Keppler et al., 2018), this can result in a homogenous distribution of AITC in the mustard particles resulting in the observed deviations.

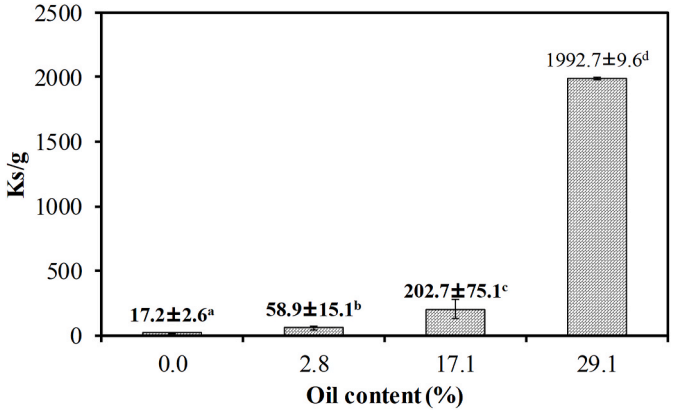

Fig. 3. Partition coefficient ($K_{s/g}$) of allyl isothiocyanate (AITC) with different fat content. *Means with the same lower case did not differ significantly at $p < 0.05$.

Overall, the model described the observed data very well. Therefore, the established multiresponse model proposed is well applicable and the reaction and mass transfer pathways (Fig. 1) in the packaging system can describe the antimicrobial active packaging system very well.

4.3. Interpretation of the estimated parameters from the established multiresponse kinetic model

The kinetic parameters and their standard deviation for this multiresponse kinetic model are summarized in Tables 1 and 2. A low-standard deviation of the parameters (Tables 1 and 2) and low parameter correlation coefficients <0.8 (Figure A4 in Supplementary Materials) were found. The effects of particle size and fat content on the estimated parameters obtained from the established kinetic model are discussed in detail below.

4.3.1. Sinigrin hydrolysis and AITC formation

The estimated kinetic parameters (the rate constants (k_1) and inaccessible sinigrin (Sin_i)) of the modified first-order model Eq. (3) are shown in Tables 1 and 2 Table 1 shows that k_1 decreased significantly with defatted particles, compared to full-fat (29.1% fat) particles as presented in Table 1 ($p < 0.05$) and Table 2 shows no significant effects of particle sizes on k_1 in general ($p > 0,05$), except for the 400-500 μm-sized defatted particles. The lower k_1 in defatted particles was not our expectation, as in our previous study it was observed that there was more cell damage in the defatted particles. A possible reason for slower k_1 is a difference in sensitivity for cell damage for different cell types. Kissen et al. (2009) have shown that sinigrin and myrosinase are located in different compartments, where myrosinase is located inside myrosin cells and sinigrin in S-cells. The fat extraction and particle reduction might not damage the myrosin cells in a similar way as the S-cells, resulting in less myrosinase release in defatted particles.

The cell damages resulted in more sinigrin being accessible to myrosinase and more AITCs are formed (Hanschen et al., 2018; Wang et al., 2011). In Tables 1 and 2 for the smallest defatted particles ($p < 0.05$) indeed less remaining sinigrin (Sin_i) after 48 h is observed. The presence of the fat in ground seeds causes its intracellular cells to remain intact as the fat content protects the cells from the grinding process, consequently, the higher sinigrin concentration was left in the ground seeds containing fat content. Additionally, a sudden increase in the inaccessible sinigrin for the big particles (400–500 and 630–800 μm) in Table 2 is likely induced by incomplete cell damage. These results confirm the previous study that observed micrographs of the big particles containing less cell damage.

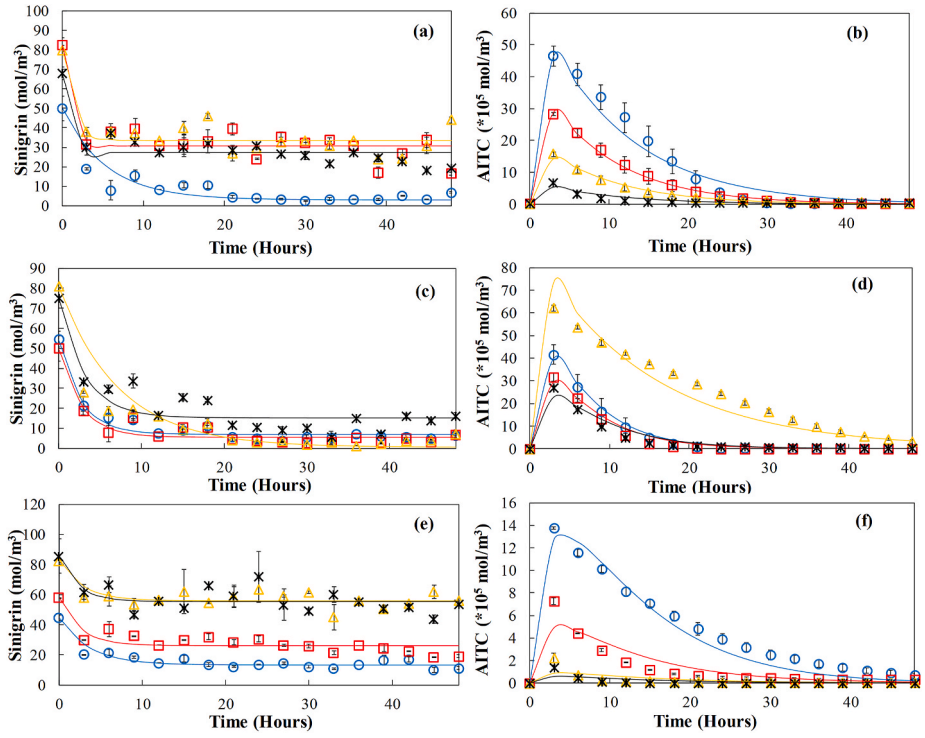

Fig. 4. Kinetic model fit (lines) to the experimental data (symbols) of sinigrin concentration (left) and AITC concentration in the headspace (right). **(a, b)** Different fat content (○: 0, □: 2.8, △:17.1, **x**:29.1%), particle sizes (200–315 μm); **(c, d)** Fat content (0%), different ranges of particle sizes (○: 50–100, □: 200–315, △:400–500, **x**:630–800 μm); **(e, f)** Fat content (29.1%), different ranges of particle sizes (○: 50–100, □: 200–315, △:400–500, **x**:630–800 μm).

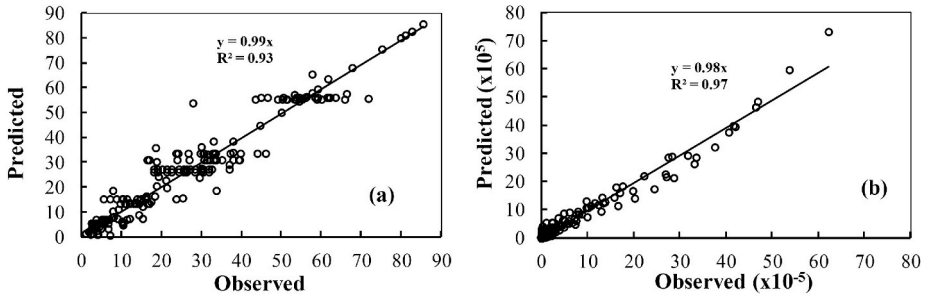

Fig. 5. Predicted against observed values for the established model for all batches of **(a)** sinigrin concentration, **(b)** allyl isothiocyanate (AITC) in the headspace. In all graphs, the units are mol/m^3.

4.3.2. AITC release from mustard particles into packaging headspace

The mass transfer kinetic model Eqs. (6) and (7) described the AITC release from mustard particles into headspace well. Tables 1 and 2 show that the mass transfer coefficient (m_t) was significantly affected by the fat content ($p < 0.05$), while no effect of particle sizes was observed ($p > 0.05$). Table 1 shows the m_t-values of the fat mustard particles (17.1 and 29.1% fat) were significantly lower than the m_t-values of the particles with lower fat content. This result was in line with the result found by Dai and Lim (2014); the release rate constants value of defatted mustard seed meal powder (MSMP) were faster than the normal MSMP. The fat in mustard particles reduced the release of AITC from the fat-particles, as the AITC was solubilized in the lipid phase (Tsao et al., 2000). As particle size did not significantly affect the AITC release, it indicates that the higher AITC concentrations observed in Fig. 4d and f were driven by the higher accessible sinigrin fraction available in the mustard seeds leading to more formation and then release of AITC into the headspace. This indicates that cell damage in the particle is crucial to make sinigrin accessible and get a higher AITC concentration in the headspace. These results may have important consequences for the formulation of mustard particle properties with controlled-release profiles of AITC and its application in the packaging.

4.3.3. AITC degradation in mustard particles and headspace

The reaction kinetics in Eqs. (8) and (9) were applied to describe AITC degradation in mustard particles and headspace, respectively. The degradation rate constant in the particles (k_2) was significantly increased in particles without fat (Tables 1 and 2) ($p < 0.05$). The high solubility of AITC in the fat phase caused the lower degradation rate of AITC in the mustard particles phase with fat. In the continuous phase (aqueous phase of particles) AITC degradation is faster, while the compounds in the dispersed phase (lipid phase) were more stable (Liu and Yang, 2010). This degradation rate of AITC in mustard particles shows that the presence of fat is the best way to stabilize the AITC concentration for a longer time.

The second-order degradation rate constant in the headspace (k_3) was estimated at around $3.02 \pm 0.30 \times 10^5$ m^3/mol.h. As no reaction

Table 1
The estimated parameters from the multiresponse kinetic model for the effect of fat content.

Fat (%)	Sizes (μm)	Parameters				
		k_1 (h^{-1})	Sin_i (mol/m^3)	k_2 ($x10^6$ m^3/mol/h)	k_3 ($x10^{-5}$ m^3/mol/h)	m_t ($x10^7$ m/h)
0.0	200–315	0.18 ± 0.02^{a}	3.12 ± 1.61^{a}	7.63 ± 1.89^{c}	3.02 ± 0.30	$186.94.\pm74.45^{c}$
2.8		0.90 ± 0.37^{ab}	30.76 ± 1.49^{c}	3.20 ± 0.27^{a}		21.40 ± 4.30^{b}
17.1		0.76 ± 0.39^{ab}	33.60 ± 1.56^{c}	3.93 ± 0.25^{b}		4.25 ± 2.21^{a}
29.1		1.96 ± 0.51^{b}	27.33 ± 0.88^{b}	3.69 ± 0.08^{ab}		0.47 ± 0.66^{a}

Values represent means ± standard deviation. Small letters indicate significant differences between particles with different fat content.

Table 2
The estimated parameters from the multiresponse kinetic model for the effect of particle size of the mustard seed particles with 0 and 29.1% fat.

Fat (%)	Sizes (μm)	Parameters				
		k_1 (h^{-1})	Sin_i (mol/m^3)	k_2 ($x10^6$ m^3/mol/h)	k_3 ($x10^{-5}$ m^3/mol/h)	m_t ($x10^7$ m/h)
0.0	50–100	0.37 ± 0.03^{b}	7.09 ± 1.48^{b}	7.63 ± 1.89^{b}	3.02 ± 0.30	20.07 ± 8.04^{a}
	200–315	0.37 ± 0.08^{b}	5.52 ± 1.58^{b}			35.80 ± 15.07^{a}
	400–500	0.14 ± 0.01^{a}	0.68 ± 1.82^{a}			$8272.12 \pm 13,048.00^{a}$
	630–800	0.32 ± 0.05^{b}	15.07 ± 1.61^{c}			44.39 ± 19.04^{a}
29.1	50–100	0.27 ± 0.03^{A}	13.45 ± 1.54^{A}	3.69 ± 0.08^{a}		2.19 ± 1.08^{A}
	200–315	0.39 ± 0.06^{AB}	26.18 ± 1.46^{B}			0.86 ± 1.10^{A}
	400–500	0.34 ± 0.04^{AB}	55.97 ± 1.46^{C}			0.06 ± 0.42^{A}
	630–800	0.43 ± 0.07^{B}	55.30 ± 1.45^{C}			0.04 ± 0.40^{A}

Values represent means ± standard deviation. Small letters indicate significant differences between the different sizes of particles with 0% fat, while capital letters indicate significant differences between the different sizes of particles with 29.1% fat.

kinetics for this reaction was described in the literature, zero-order, first-order, fractional conversion first-order, and second-order kinetics were tried to fit the experimental data of the headspace AITC concentration. When fitting the model to the experimental data, only the second-order model in Eq. (9) can adequately describe the AITC degradation in the headspace without a trend in the residuals and an estimated parameter with a low standard deviation.

The effectiveness of AITC as an antimicrobial agent relies on its concentration in the packaging system (Dufour et al., 2015; Saladino et al., 2017). Once the concentration of AITC in the packaging system is lower than its minimum inhibitory concentration (MIC) against certain bacteria, the bacteria will grow and spoil the foods. AITC degradation is accounted for its stability to maintain the capability of AITC to keep the inhibition of bacteria. The breakdown products of AITC, e.g. allyl-dithiocarbamate and pentasulfide have no antimicrobial activity (Tsao et al., 2000; Weerawatanakorn et al., 2015), so besides the controlled release of AITC in the packaging system, the rate of degradation in the packaging system needs to be hindered to maintain the concentration above MIC. Further study related to other factors reducing the AITC degradation in the headspace, like temperature (Saladino et al., 2017), is required to retain AITC in the headspace to have a longer antimicrobial inhibition in foods.

5. Conclusion

The multiresponse kinetic model combining the mechanisms of (bio) chemical reactions and mass transfer of AITC inside the packaging system described the experimental observations well. This model produced a good prediction of the enzymatic hydrolysis of sinigrin, AITC formation, its release, and degradation in the mustard particle and headspace. Defatting the mustard particles has positive impacts on some parameters, e.g. increasing the accessible sinigrin and lowering the formation rate constant and increasing the mass transfer coefficient between the particles and the headspace. The particle size has a small effect on the estimated parameters, and no significant effect on the release of AITC into the headspace was found. The results also confirm our previous study that fat content has a significant effect on the partitioning of AITC in the packaging system. The better understanding of the kinetics of the concurrent reactions and mass transfer in the packaging system by this study can help to optimize the mustard seeds properties to effectively control the AITC release for antimicrobial packaging design. A similar multiresponse modelling approach as described in this paper can be applied for future applications, with other components used in the active packaging concept.

CRediT authorship contribution statement

Nur Alim Bahmid: Conceptualization, Methodology, Software, Investigation, Data curation, Visualization, Formal analysis, Writing - original draft, Funding acquisition. **Jenneke Heising:** Conceptualization, Supervision, Writing - review & editing. **Matthijs Dekker:** Conceptualization, Software, Formal analysis, Supervision, Writing - review & editing.

Declaration of competing interests

The authors declare that they have no known competing financial interests or personal relationships that could have appeared to influence the work reported in this paper.

Acknowledgment

This work is supported by the Indonesian Endowment Fund for Education (LPDP) (Grant numbers: PRJ-4174/LPDP.3/2016).

Appendix A. Supplementary data

Supplementary data to this article can be found online at https://doi.org/10.1016/j.jfoodeng.2020.110370.

References

Backhurst, J.R., Harker, J.H., 2001. Section 10 - mass transfer. In: Backhurst, J.R., Harker, J.H. (Eds.), Chemical Engineering. Butterworth-Heinemann, Oxford, pp. 217–284.
Bahmid, N.A., Pepping, L., Dekker, M., Fogliano, V., Heising, J., 2020. Using particle size and fat content to control the release of Allyl isothiocyanate from ground mustard seeds for its application in antimicrobial packaging. Food Chem. 308.
Boekel, M.A.J.S.v., 2009. Kinetic Modeling of Reactions in Foods. CRC Press, Boca Raton.
Dai, R.Y., Lim, L.T., 2014. Release of allyl isothiocyanate from mustard seed meal powder. J. Food Sci. 79 (1), E47–E53.

Dekker, M., Hennig, K., Verkerk, R., 2009. Differences in thermal stability of glucosinolates in five Brassica vegetables. Czech J. Food Sci. 27 (Special Issue), S85–S88.
Dufour, V., Stahl, M., Baysse, C., 2015. The antibacterial properties of isothiocyanates. Microbiology 161 (2), 229–243.
Encinas-Basurto, D., Ibarra, J., Juarez, J., Burboa, M.G., Barbosa, S., Taboada, P., Troncoso-Rojas, R., Valdez, M.A., 2017. Poly(lactic-co-glycolic acid) nanoparticles for sustained release of allyl isothiocyanate: characterization, in vitro release and biological activity. J. Microencapsul. 34 (3), 231–242.
Goncuoglu Tas, N., Gokmen, V., 2017. Maillard reaction and caramelization during hazelnut roasting: a multiresponse kinetic study. Food Chem. 221, 1911–1922.
Hanschen, F.S., Kühn, C., Nickel, M., Rohn, S., Dekker, M., 2018. Leaching and degradation kinetics of glucosinolates during boiling of Brassica oleracea vegetables and the formation of their breakdown products. Food Chem. 263, 240–250.
Harrison, M., Hills Brian, P., Bakker, J., Clothier, T., 2006. Mathematical models of flavor release from Liquid emulsions. J. Food Sci. 62 (4), 653–664.
Jiang, Z.T., Zhang, Q.F., Tian, H.L., Li, R., 2006. The reaction of allyl isothiocyanate with hydroxyl/water and beta-cyclodextrin using ultraviolet spectrometry. Food Technol. Biotechnol. 44 (3), 423–427.
Julious, S.A., 2004. Using confidence intervals around individual means to assess statistical significance between two means. Pharmaceut. Stat. 3 (3), 217–222.
Keppler, J.K., Steffen-Heins, A., Berton-Carabin, C.C., Ropers, M.-H., Schwarz, K., 2018. Functionality of whey proteins covalently modified by allyl isothiocyanate. Part 2: influence of the protein modification on the surface activity in an O/W system. Food Hydrocolloids 81, 286–299.
Kissen, R., Rossiter, J.T., Bones, A.M., 2009. The 'mustard oil bomb': not so easy to assemble?! Localization, expression and distribution of the components of the myrosinase enzyme system. Phytochemistry Rev. 8 (1), 69–86.
Kocadağlı, T., Gökmen, V., 2016. Multiresponse kinetic modelling of Maillard reaction and caramelisation in a heated glucose/wheat flour system. Food Chem. 211, 892–902.
Kurek, M., Laridon, Y., Torrieri, E., Guillard, V., Pant, A., Stramm, C., Gontard, N., Guillaume, C., 2017. A mathematical model for tailoring antimicrobial packaging material containing encapsulated volatile compounds. Innovat. Food Sci. Emerg. Technol. 42, 64–72.
Liu, T.T., Yang, T.S., 2010. Stability and antimicrobial activity of allyl isothiocyanate during long-term storage in an oil-in-water emulsion. J. Food Sci. 75 (5), C445–C451.
Lorenzo, J.M., Batlle, R., Gómez, M., 2014. Extension of the shelf-life of foal meat with two antioxidant active packaging systems. LWT - Food Sci. Technol. (Lebensmittel-Wissenschaft -Technol.) 59 (1), 181–188.
Lüthy, B., Matile, P., 1984. The mustard oil bomb: rectified analysis of the subcellular organisation of the myrosinase system. Biochem. Physiol. Pflanz. (BPP) 179 (1), 5–12.
Nakano, R.T., Yamada, K., Bednarek, P., Nishimura, M., Hara-Nishimura, I., 2014. ER bodies in plants of the Brassicales order: biogenesis and association with innate immunity. Front. Plant Sci. 5, 73.
Okunade, O.A., Ghawi, S.K., Methven, L., Niranjan, K., 2015. Thermal and pressure stability of myrosinase enzymes from black mustard (Brassica nigra L. WDJ Koch. var. nigra), brown mustard (Brassica juncea L. Czern. var. juncea) and yellow mustard (Sinapsis alba L. subsp maire) seeds. Food Chem. 187, 485–490.
Olaimat, A.N., Holley, R.A., 2016. Inhibition of Listeria monocytogenes on cooked cured chicken breasts by acidified coating containing allyl isothiocyanate or deodorized Oriental mustard extract. Food Microbiol. 57, 90–95.
Oliviero, T., Verkerk, R., Dekker, M., 2012. Effect of water content and temperature on glucosinolate degradation kinetics in broccoli (Brassica oleracea var. italica). Food Chem. 132 (4), 2037–2045.
Quintas, M., Guimarães, C., Baylina, J., Brandão, T.R.S., Silva, C.L.M., 2007. Multiresponse modelling of the caramelisation reaction. Innovat. Food Sci. Emerg. Technol. 8 (2), 306–315.
Quintavalla, S., Vicini, L., 2002. Antimicrobial food packaging in meat industry. Meat Sci. 62 (3), 373–380.
Reyes-Jurado, F., Cervantes-Rincón, T., Bach, H., López-Malo, A., Palou, E., 2019. Antimicrobial activity of Mexican oregano (Lippia berlandieri), thyme (Thymus vulgaris), and mustard (Brassica nigra) essential oils in gaseous phase. Ind. Crop. Prod. 131, 90–95.
Saladino, F., Bordin, K., Luciano, F.B., Franzón, M.F., Mañes, J., Meca, G., 2017. Antimicrobial activity of the glucosinolates. In: Mérillon, J.-M., Ramawat, K.G. (Eds.), Glucosinolates. Springer International Publishing, Cham, pp. 249–274.
Stauber, E.J., Kuczka, P., van Ohlen, M., Vogt, B., Janowitz, T., Piotrowski, M., Beuerle, T., Wittstock, U., 2012. Turning the 'mustard oil bomb' into a 'cyanide bomb': aromatic glucosinolate metabolism in a specialist insect herbivore. PloS One 7 (4), e35545.
Tetteh, O.N.A., Ulrichs, C., Huyskens-Keil, S., Mewis, I., Amaglo, N.K., Oduro, I.N., Adarkwah, C., Obeng-Ofori, D., Förster, N., 2019. Effects of harvest techniques and drying methods on the stability of glucosinolates in Moringa oleifera leaves during post-harvest. Sci. Hortic. 246, 998–1004.
Torrijos, R., Nazareth, T.M., Perez, J., Manes, J., Meca, G., 2019. Development of a bioactive sauce based on oriental mustard flour with antifungal properties for pita bread shelf life improvement. Molecules 24 (6).
Tsao, R., Yu, Q., Friesen, I., Potter, J., Chiba, M., 2000. Factors affecting the dissolution and degradation of oriental mustard-derived sinigrin and allyl isothiocyanate in aqueous media. J. Agric. Food Chem. 48 (5), 1898–1902.
Verkempinck, S.H.E., Salvia-Trujillo, L., Infantes Garcia, M.R., Hendrickx, M.E., Grauwet, T., 2019. From single to multiresponse modelling of food digestion kinetics: the case of lipid digestion. J. Food Eng. 260, 40–49.
Wang, T.X., Liang, H., Yuan, Q.P., 2011. Optimization of ultrasonic-stimulated solvent extraction of sinigrin from Indian mustard seed (Brassica juncea L.) using response surface methodology. Phytochem. Anal. 22 (3), 205–213.
Weerawatanakorn, M., Wu, J.C., Pan, M.H., Ho, C.T., 2015. Reactivity and stability of selected flavor compounds. J. Food Drug Anal. 23 (2), 176–190.
Wong, L.-W., Hou, C.-Y., Hsieh, C.-C., Chang, C.-K., Wu, Y.-S., Hsieh, C.-W., 2020. Preparation of antimicrobial active packaging film by capacitively coupled plasma treatment. LWT 117.
Xiao, Z., Rausch, S.R., Luo, Y., Sun, J., Yu, L., Wang, Q., Chen, P., Yu, L., Stommel, J.R., 2019. Microgreens of Brassicaceae: genetic diversity of phytochemical concentrations and antioxidant capacity. LWT 101, 731–737.
Zhang, Z.-Q., Kim, W.-T., Park, Y.-C., Chung, D., 2010. Thermodynamics of partitioning of allyl isothiocyanate in oil/air, oil/water, and octanol/water systems. J. Food Eng. 96 (4), 628–633.
Ziegel, E.R., Gorman, J.W., 1980. Kinetic modelling with multiresponse data. Technometrics 22 (2), 139–151.